Electronic Supplementary Material (ESI) for ChemComm.

Supporting Information

Construction of hierarchical membrane with angstrom-scale ion channels for enhanced Li^+/Mg^{2+} separation

Lin Fu,[‡ab] Qingchen Wang,[‡ab] Yuhao Hu,[ab] Yongchao Qian,[a] Weiwen Xin,[ab] Shengyang Zhou,[a] Xiang-Yu Kong,[*abc] and Liping Wen[*abc]

[a]Key Laboratory of Bio-inspired Materials and Interfacial Science, Technical Institute of Physics and Chemistry, Chinese Academy of Sciences, Beijing 100190, P. R. China.
[b]School of Future Technology, University of Chinese Academy of Sciences, Beijing 100049, P. R. China.
[c]Binzhou Institute of Technology，Binzhou 256600, P. R. China

Materials & Methods

Materials

MXene dispersion (5 mg mL^{-1}) was purchased from Feynman Biotechnology Co., Ltd. Phytic acid, zinc acetate and 2-Methylimidazole were purchased from Aladdin. LiCl (>99.5%) and $MgCl_2$ (>99.5%) were purchased from Sigma-Aldrich. anhydrous methanol and anhydrous ethanol were purchased from Sinopharm Chemical Reagent Co., Ltd. All the above chemicals were used without further purification. All deionized water used in the experiments was produced by the Milli-Q ultrapure water system.

Methods

Preparation of ZIF-8/MXene membrane

As shown in Scheme. 1, the ZIF-8/MXene hierarchical membrane was synthesized by the phytic acid-assisted electrochemical deposition method. Firstly, a thickness of ≈7.5 μm MXene membrane was obtained simply by vacuum filtration (Fig. S1 and S3). The $Ti_3C_2T_x$ solution is dispersed in DI water with a concentration of 1 mg mL^{-1}, following 10-minutes sonication. Then a certain amount of dispersed $Ti_3C_2T_x$ nanosheets is assembled into a nanofluidic membrane upon vacuum filtration on a polycarbonate (PC, an average pore size of 200 nm), and the free-standing membrane can be exfoliated from substrates after drying. The MXene membrane was immersed in phytic acid (PA) solution for surface modification for 15 min to obtain the PA-MXene membrane. The concentration of phytic acid solution was 10 mg ml^{-1} with anhydrous ethanol as the solvent. The precursor solution for the subsequent electro-deposition was prepared: 1.536 g zinc acetate was dissolved in 70 mL anhydrous methanol as solution A; 1.149 g 2-methylimidazole was dissolved in 70 mL anhydrous methanol as solution B. The equal volume of solution A and solution B were mixed uniformly to obtain the electro-deposition mother solution. The PA-MXene membrane was immerged into the mother solution prepared as stated above. The ZIF-8/MXene membrane was synthesized by electrochemical deposition method. A current density of -0.64 mA cm^{-2} was conducted for a certain period (30 min) at room temperature to generate the ZIF-8 layer on the MXene before the membranes were taken out and dried at room temperature. The ZIF-8/MXene membrane with hierarchical structure contains ultrasmall nanochannel, that is angstrom-sized windows of the ZIF-8 layer endow the membrane with enhanced ion-sieving properties for Li+/Mg2+. Meanwhile, the nanometer-size cavities of ZIF-8 and interlayer channels of MXene are the larger channels of the ZIF-8/MXene membrane, which function as ion transport pathways, achieving fast and selective transport of Li-ions.

Characterizations

SEM (Hitachi S-4800 (Japan)) was used to observe the surface and sectional structure of the MXene membranes and ZIF-8/MXene hierarchical membranes at 10 kV. Energy dispersive X-ray spectroscopy (EDS) mappings were used to explore the element distribution of the membranes. X-ray diffraction (XRD) (D8 focus) with a Cu Kα radiation source (λ = 1.54181 Å, 40 kV, and 30 mA) was used to characterize the crystallography characteristics of MXene membrane and ZIF-8/MXene membrane. X-ray photoelectron spectroscopy (XPS) spectra were collected on an Al Kα source (ESCALAB 250Xi).

Electrical measurements

Keithley 6487 picoammeter (Keithley Instruments, Cleveland, OH) was used to record the ionic

current through the membranes. The Current-Voltage (I-V) curves were measured by the Ag/AgCl electrodes. During the tests, the membranes were sandwiched between two cells containing electrolytes. The efficient membrane area was about 3.14 mm^2 and the sweeping voltage was from -0.2 V to +0.2 V with a step of 0.02 V. The ion conductance of membrane is derived from corresponding I-V curves. To accurately determine the contribution of the membrane in ion sieving, the conductance (G_M) calculated without R_S could reflect the intrinsic ion transport property of the membrane. The G_M could be estimated by rearranging as:

$$G_M = \frac{1}{R_M} = \frac{1}{R_T - 2 \times R_S} \quad (1)$$

G_M is the inherent ion conductance, R_M is membrane resistance, R_s is solution resistance, and R_T is total resistance. The selectivity ratio (α), also inherent ion selectivity, was defined as:

$$\alpha = \frac{G_M(Li^+)}{G_M(Mg^{2+})} \quad (2)$$

$G_M(Li^+)$ and, $G_M(Mg^{2+})$ are the ion conductance of membrane in 0.01 M LiCl solution and 0.01 M $MgCl_2$ solution, respectively.

Ion permeation testing

First, the hierarchical membrane sealed by the rubber gasket was placed in the middle of the homemade permeation setup. The feed side was the equal concentrations of metallic salt mixed solution or natural brine. The permeation side was filled with an equal volume of DI water (resistivity: 18.2 MΩ), and stirring to prevent concentration polarization. The metal ions concentrations in the permeation compartment were measured by ICP-MS (PerkinElmer 1000G) to calculate the ions flux and ion selectivity using the following expression:[1]

$$J = \frac{(C_f - C_i) \cdot V}{A_m \cdot t} \quad (3)$$

J is the metal ion flux (mmol m^{-2} h^{-1}), C_f and C_i are the metal ion concentration in the recovery compartment at the final time and initial moment, V is the volume of recovery solution, A_m is the effective area of the hierarchical membrane, and t is the time corresponding to ion transmembrane transport. Ion selectivity is defined as:

$$\eta = \frac{J_{Li}}{J_{Mg}} \quad (4)$$

η is ion selectivity, J_{Li} is the ion flux of Li ions, and J_M is the ion flux of Mg ions. The perm-selectivity of the membrane could be calculated from:[2]

$$P_{Mg^{2+}}^{Li^+} = \frac{J_{Li} C_{Mg}}{J_{Mg} C_{Li}} \quad (5)$$

Where P refers to the perm-selectivity of Li^+/Mg^{2+}, C refers to the concentration of Li^+ and Mg^{2+} in the feed solution.

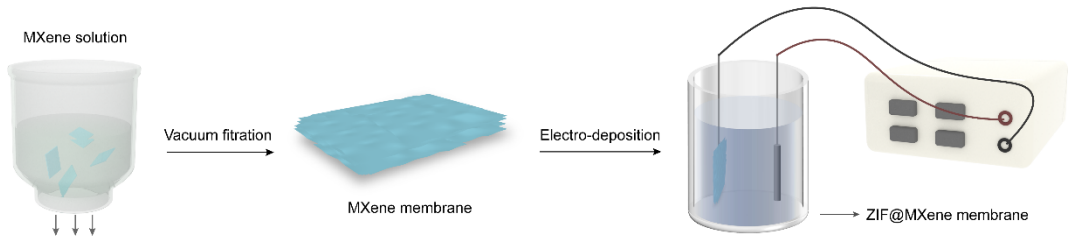

Fig. S1 The synthesis scheme of the ZIF-8/MXene hierarchical membrane. The MXene membrane was fabricated by the vacuum filtration process. Subsequently, the MXene membrane was immersed in phytic acid, and then the ZIF-8 layer was electro-deposited onto the PA-modified MXene membrane.

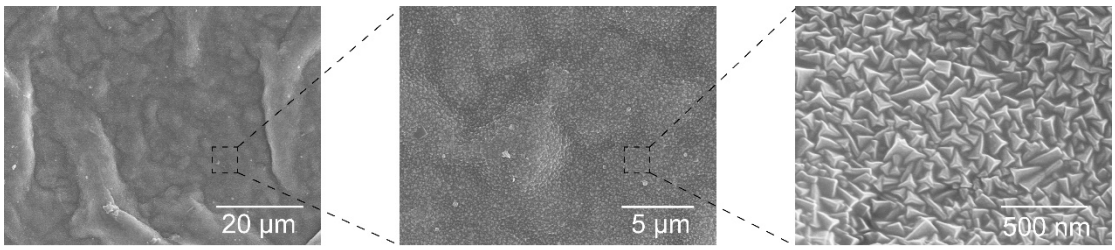

Fig. S2 The SEM images with different resolutions showed that ZMM was fully covered by a compact and continuous polycrystal ZIF-8 layer.

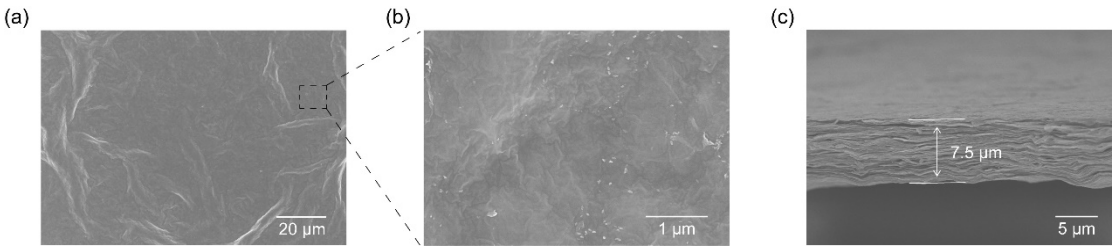

Fig. S3 (a) The SEM image of the surface of the pristine MXene substrates and (b) corresponding enlarged image. (c) The cross-sectional SEM image of the pristine MXene substrates. The MXene showed a smooth surface and a thickness of about 7.5 μm.

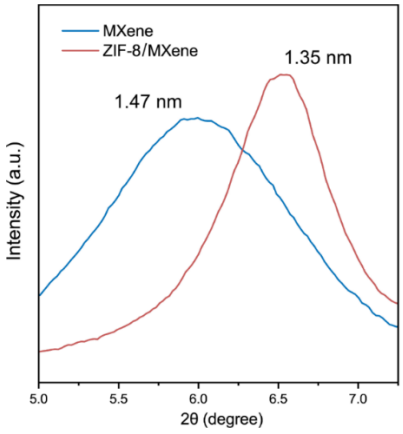

Fig. S4 XRD patterns of pristine MXene membrane and MXene side of the hierarchical ZIF-8/MXene membrane at the diffraction peak (002). The XRD characterization showed that the width of diffraction peak got narrow after electro-deposition, indicating the more ordered interlayer ion channels which could promote the ion transport. In addition, the interlayer spacing was decreased from 1.47 nm to 1.35 nm, which could be linked to the tighter assembly of the nanosheets, endowing the membrane with working stability in water condition.

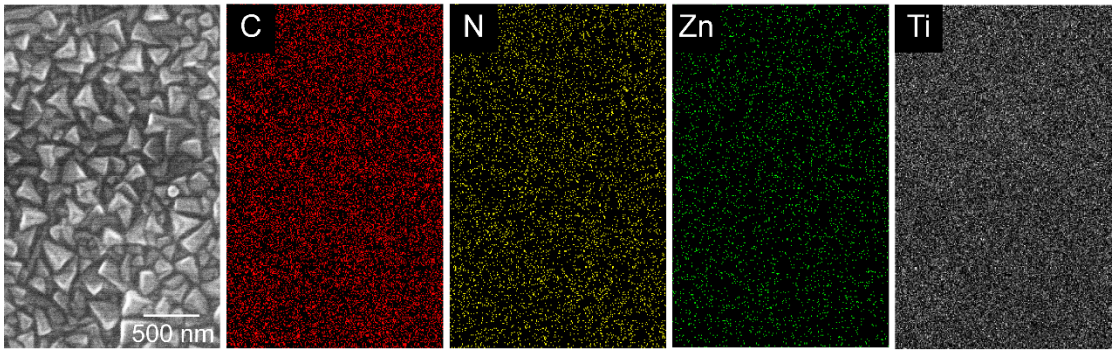

Fig. S5 SEM image and EDS spectra of the surface of the ZMM. The elements of C, N, Zn and Ti could be observed in the ZMM, indicating the MXene substrate was fully covered by the ZIF-8 layer

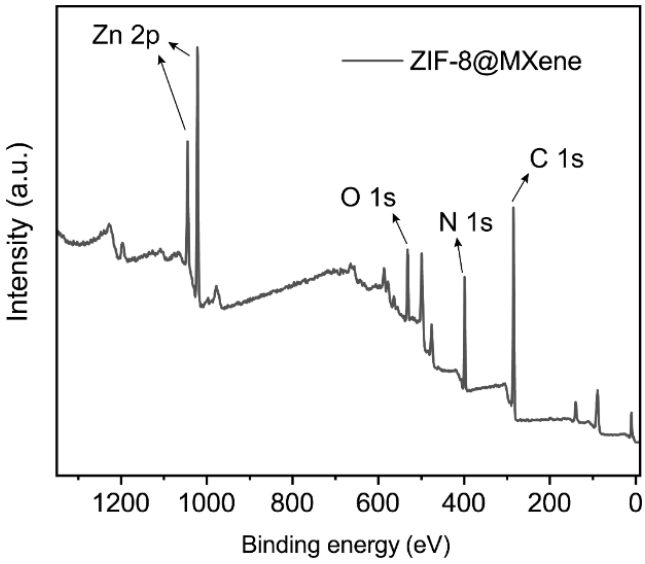

Fig. S6 XPS spectrum of the ZMM. The elements of Zn, O, N, and C could be observed, confirming that the ZIF-8 was deposited in the ZMM.

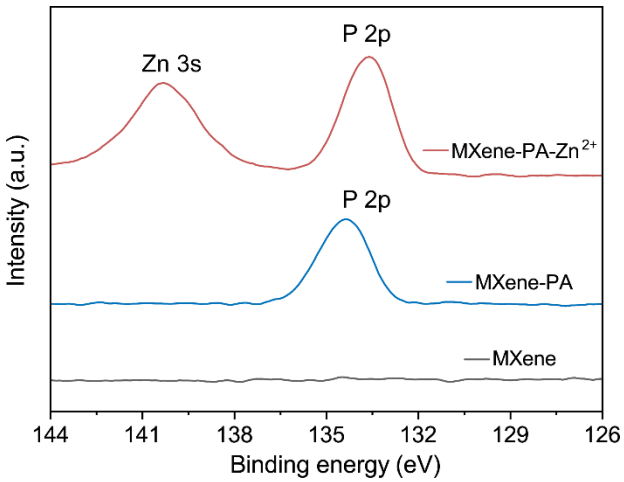

Fig. S7 XPS spectra of the Zn 3s and P 2p region of the pristine MXene membrane, phytic acid-coated MXene membrane and ZIF-8/MXene membrane after washing by ICP. There was no Zn element observed in the pristine MXene membrane and the PA-MXene membrane, indicating that the ZIF-8 could be modified in the MXene membrane stably by the electrochemical deposition.

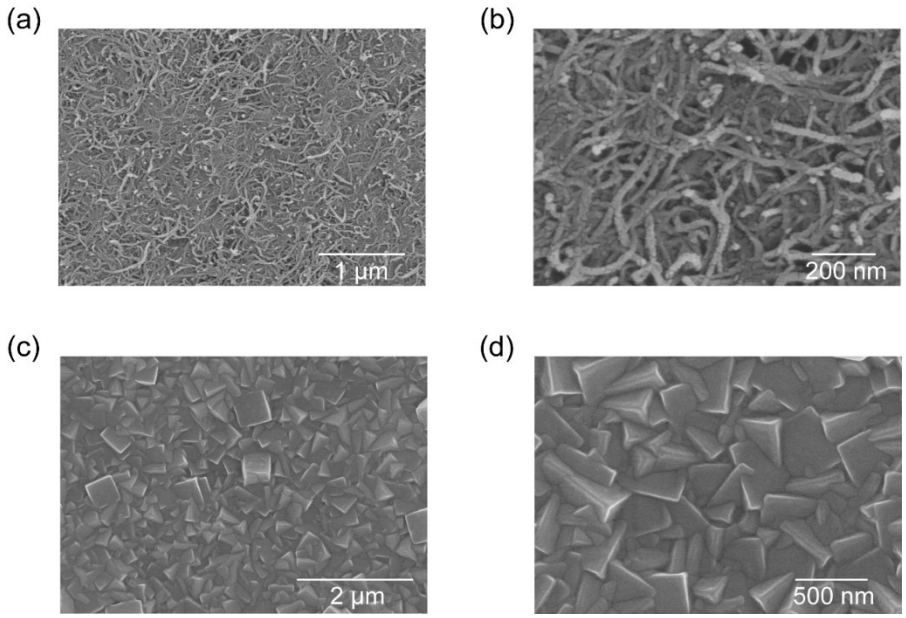

Fig. S8 The surface SEM images of (a, b) CNT membrane, and (c, d) ZIF-8/CNT hierarchical membrane. As shown in Fig. S7a-b, the as-prepared CNT membrane was interwoven by numerous nanotube fibres and the gaps formed by the stacked neighbouring nanotubes constituted ion-transporting pores. And the ZIF-8/CNT membranes displayed a compact surface covered fully by the polycrystal ZIF-8 layer.

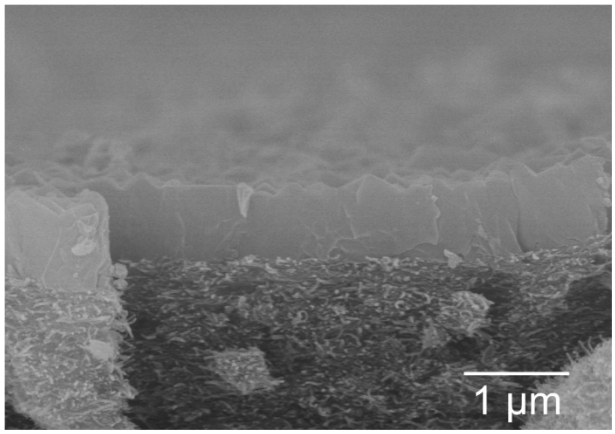

Fig. S9 The cross-sectional SEM image of ZIF-8/CNT hierarchical membrane. A ZIF-8 layer with a thickness of about 630 nm was densely deposited on the top of the CNT substrate.

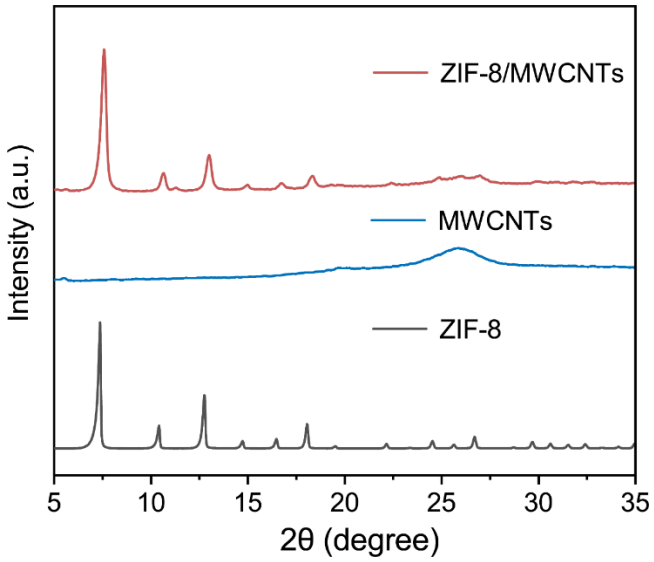

Fig. S10 XRD patterns of the ZIF-8/CNT hierarchical membrane, pristine CNT membrane and ZIF-8. The XRD patterns of the ZMM demonstrated that the as-prepared membrane was modified successfully with a polycrystal ZIF-8 layer.

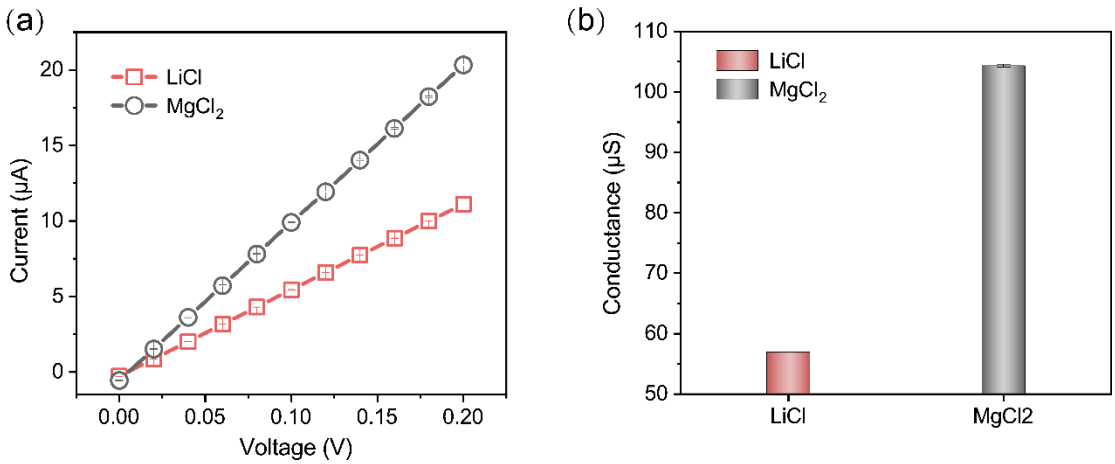

Fig. S11 (a) The bulk *I-V* curves and (b) conductance of the LiCl and $MgCl_2$ solutions (0.01M).

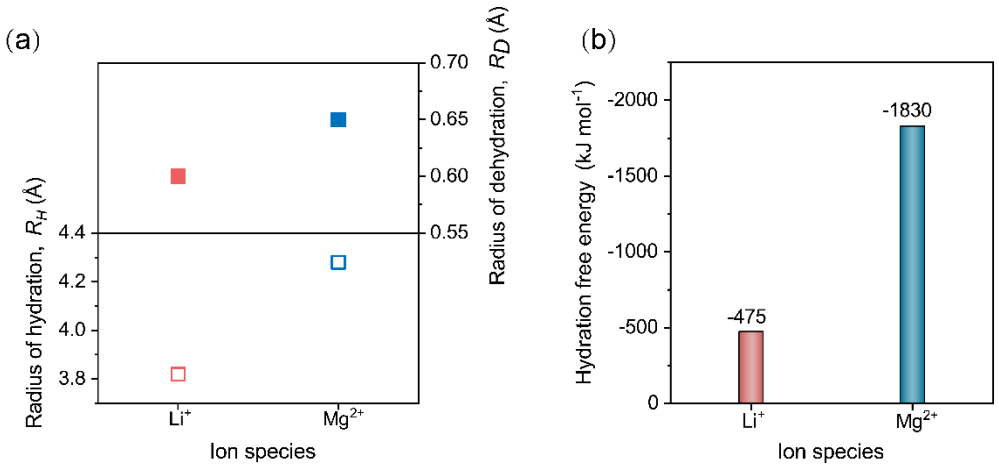

Fig. S12 (a) The radius of hydration (right y-axis) and the bare radius (left y-axis) of the Li^+ and Mg^{2+}. (b) The hydration free energy of Li^+ and Mg^{2+}.

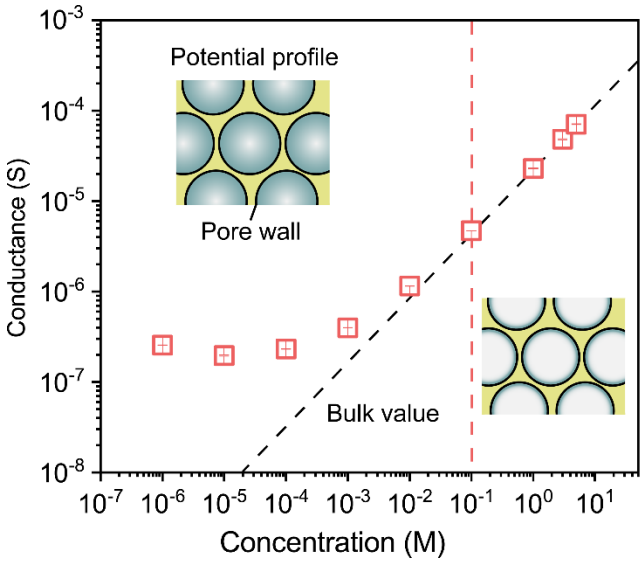

Fig. S13 Ion conductance of ZMM under different concentrations of LiCl solutions. The ion conductance increased paradoxically at the low concentration, indicating the surface-charge-governed ion transport.

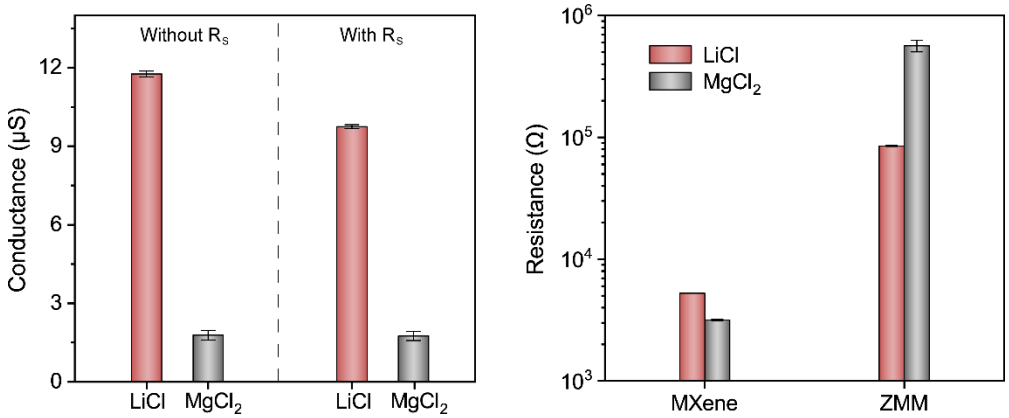

Fig. S14 (a) The total resistance (measured value) and individual resistance of the hierarchical membrane (ZMM) according to the electrochemical model. (b) The ion conductance of the MM and ZMM.

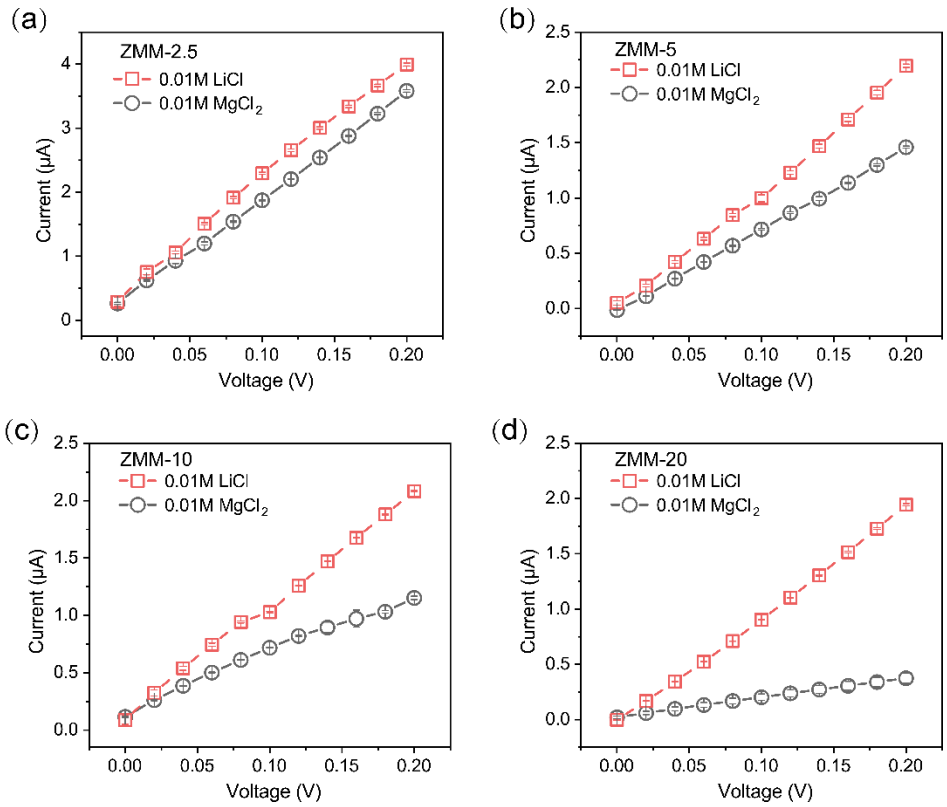

Fig. S15 (a-d) The *I-V* curves measured in LiCl and $MgCl_2$ solutions (0.01M) of the hierarchical membrane prepared with different cut-off voltage of 2.5 V, 5V, 15V and 20V, respectively. The corresponding ionic conductance could be calculated based on the *I-V* curves, from which further analysis on ion sieving properties could be conducted.

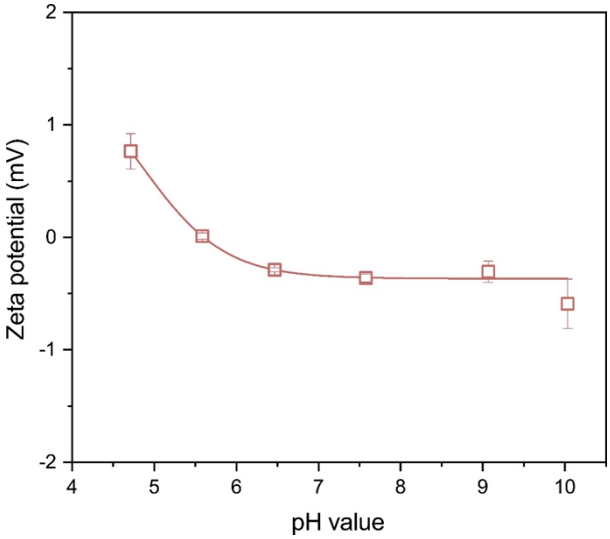

Fig. S16 Zeta potential of the ZIF-8/MXene membrane. The membrane surface of the ZIF-8 side is the measured surface. The Zeta potential of ZIF-8 decreased with increasing pH and then tended to be horizontal, remaining at ~-0.5 mV. The low surface charge of the ZIF-8 indicates that the Donnan effect has little effect on the ion separation, which is mainly based on the size-exclusion effect.

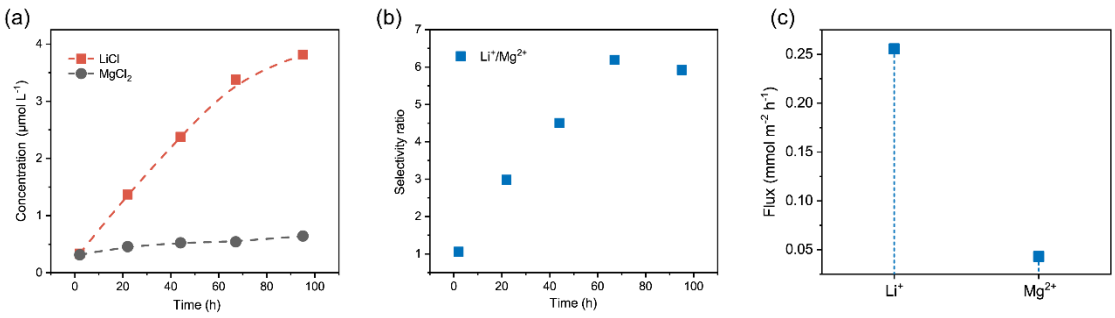

Fig. S17 The ion penetration experiments (The feed solution is mixed LiCl and $MgCl_2$ with equal concentration of 0.005 M). (a) The ion concentration in the received solution. (b) The Li^+/Mg^{2+} selectivity of the hierarchical membrane. (c) The ion flux of the hierarchical membrane. The Li^+/Mg^{2+} selectivity of ZMM in the mixed solution of lower concentration achieved a value about 6.2, higher than in the high concentration solutions, reflecting its promising perspective of application in the sea water.

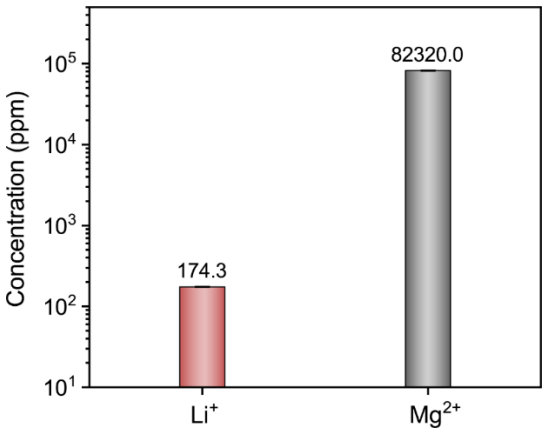

Fig. S18 The ion concentration of the real brine. The content of Mg^{2+} was several orders of magnitude higher than the content of Li^+, that the Li^+/Mg^{2+} ratio in this brine could achieve a value up to 0.0021.

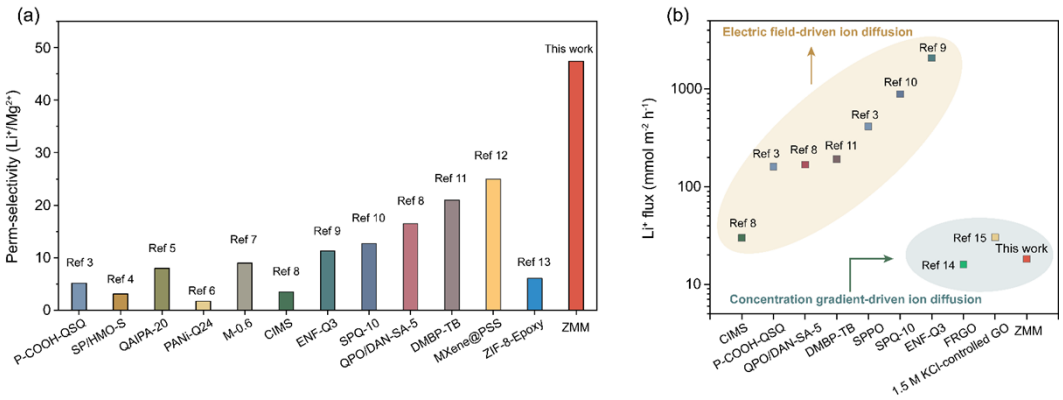

Fig. S19 (a) Comparison of the perm-selectivity of the ZMM and other reported separation systems. (b) Comparison of the Li^+ flux of the ZMM and other reported separation systems. The ion permeation test has proved the Li^+/Mg^{2+} sieving performance of the hierarchical ZIF-8/MXene membrane. The Li^+ fluxes driven by concentration gradient were lower than that driven by electric field mainly because ions are subjected to a stronger driving force under the electric field.[3-15]

References

1. W. Wang, Y. Zhang, M. Tan, C. Xue, W. Zhou, H. Bao, C. Hon Lau, X. Yang, J. Ma and L. Shao, *Sep. Purif. Technol.*, 2022, **297**, 121520.
2. F. Sheng, N. U. Afsar, Y. Zhu, L. Ge and T. Xu, *Membranes*, 2020, **10**, 114.
3. N. U. Afsar, M. A. Shehzad, M. Irfan, K. Emmanuel, F. Sheng, T. Xu, X. Ren, L. Ge and T. Xu, *Desalination*, 2019, 458, 25-33.
4. J. Zhang, X. Cui, F. Yang, L. Qu, F. Du, H. Zhang and J. Wang, *Macromol. Mater. Eng.*, 2019, 304, 1800567.
5. N. Ul Afsar, X. Ge, Z. Zhao, A. Hussain, Y. He, L. Ge and T. Xu, *Sep. Purif. Technol.*, 2021, 254, 117619.
6. X. Pang, Y. Tao, Y. Xu, J. Pan, J. Shen and C. Gao, *J. Membr. Sci.*, 2020, 595, 117544.
7. L. Tao, X. Wang, F. Wu, B. Wang, C. Gao and X. Gao, *Sep. Purif. Technol.*, 2022, 296, 121309.
8. M. Irfan, T. Xu, L. Ge, Y. Wang and T. Xu, *J. Membr. Sci.*, 2019, 588, 117211.
9. F. Sheng, L. Hou, X. Wang, M. Irfan, M. A. Shehzad, B. Wu, X. Ren, L. Ge and T. Xu, *J. Membr. Sci.*, 2020, 594, 117453.
10. N. U. Afsar, W. Ji, B. Wu, M. A. Shehzad, L. Ge and T. Xu, *Desalination*, 2019, 472, 114145.
11. J. Zhou, Z. Jiao, Q. Zhu, Y. Li, L. Ge, L. Wu, Z. Yang and T. Xu, *J. Membr. Sci.*, 2021, 627, 119246.
12. Z. Lu, Y. Wu, L. Ding, Y. Wei and H. Wang, *Angew. Chem. Int. Ed.*, 2021, 60, 22265-22269.
13. C. Qi, J. Li, Y. Shi, B. Zhang, T. Chen, C. Wang, Q. Liu and X. Yang, *J. Solid State Chem.*, 2022, 313, 123281.
14. Y.-H. Xi, Z. Liu, J. Ji, Y. Wang, Y. Faraj, Y. Zhu, R. Xie, X.-J. Ju, W. Wang, X. Lu and L.-Y. Chu, *J. Membr. Sci.*, 2018, 550, 208-218.
15. S. Wang, S. Liang, L. Chen, L. Mu, G. Xu and H. Fang, *Chem. Commun.*, 2020, 56, 2743-2746.